

Nested Bayesian Optimization for Computer Experiments

Yan Wang, Meng Wang, Areej AlBahar, Xiaowei Yue, *IEEE Senior Member*

Abstract—Computer experiments can emulate the physical systems, help computational investigations, and yield analytic solutions. They have been widely employed with many engineering applications (e.g., aerospace, automotive, energy systems). Conventional Bayesian optimization did not incorporate the nested structures in computer experiments. This paper proposes a novel nested Bayesian optimization for complex computer experiments with multi-step or hierarchical characteristics. We prove the theoretical properties about nested outputs given two cases: Gaussian or non-Gaussian. The closed forms of nested expected improvement are derived. We also propose the computational algorithms for nested Bayesian optimization. Three numerical studies show that the proposed nested Bayesian optimization outperforms the five benchmark Bayesian optimization methods ignoring the intermediate outputs of the inner computer code. The case study shows that the nested Bayesian optimization can efficiently minimize the residual stress during composite structures assembly and avoid convergence to the local optimum.

Index Terms—Nested Computer Experiment, Bayesian Optimization, Gaussian Process, Surrogate Modeling, Multistage Manufacturing

I. INTRODUCTION

COMPUTER experiments have become increasingly used in engineering simulations as the development of information technology and computing powers. Especially for the scenarios where physical experiments are difficult, expensive, or impossible to implement, computer experiments can serve as proxy surrogates for and adjuncts to physical experiments [1]. In advanced manufacturing and mechatronics, typical computer experiments may rely on Finite Element Analysis (FEA), Computational Fluid Dynamics (CFD), multiphysics simulation, variation propagation analysis, etc. Widely used engineering simulation software includes ANSYS, Matlab/Simulink, COMSOL Multiphysics, Solidworks, 3DCS. Sophisticated computer codes can model the multi-step or multi-physics processes accurately, thereby improving the efficiency of engineering design, system optimization, and quality control.

Manuscript received XX, 2021; revised XX, 2021. (*Corresponding author: Xiaowei Yue*). Dr. Yue's research was supported by the National Science Foundation (2035038); Dr. Wang's research was supported by the Natural Science Foundation of Beijing Municipality (1214019).

Y. Wang and M. Wang are with the School of Statistics and Data Science, Faculty of Science, Beijing University of Technology, Beijing 100124, China. (e-mail: yanwang@bjut.edu.cn)

A. AlBahar and X. Yue are with the Grado Department of Industrial and Systems Engineering, Virginia Tech, Blacksburg, VA, 24061 USA (e-mail: areejaa3@vt.edu; xwy@vt.edu)

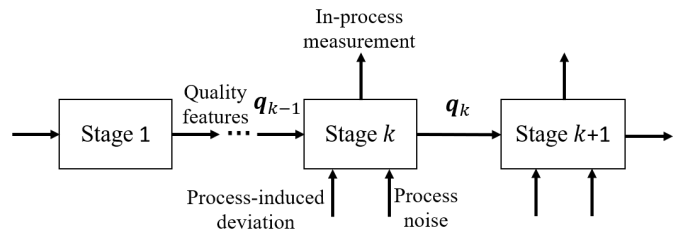


Fig. 1. Variation Propagation in Multistage Manufacturing Systems.

A. Nested Computer Experiments

Firstly, we will illustrate what is *nested computer experiment*, and why the nested effect is very critical for engineering simulations, in particular for advanced manufacturing. If one model or system contains the outputs of the other model or system, we call them *nested*. Nested property usually comes from the hierarchical structures of systems and multiphysics phenomena. In practice, one system often contains a few subsystems; the output of one subsystem could be the input for the sequential subsystem. Nested structures are ubiquitous in engineering simulation. Suppose one computer experiment includes multi-layer sequential operations/codes, and outputs from one computer code may serve as the inputs for the other level of computer code. In that case, we call it a nested computer experiment. The *nested computer experiment codes* are also called *System of Solvers* in engineering.

Most computer simulations and digital twins for multistage manufacturing processes (MMP) are nested, because of the natural multi-step structure and inherent hierarchy in advanced manufacturing systems. In MMP, multiple operations/stations are involved to produce one product [2], as shown in Fig. 1. The product quality variations can propagate from one station to its downstream station. Stream of Variation methodologies have been developed to model and reduce the variation and improve the quality control [2]–[5]. When simulating the MMP in Fig. 1, the inputs for stage k include two types: input quality features q_{k-1} from the upstream stage $k-1$, and the new process-induced deviations and noise at the current stage. Similarly, the outputted quality features q_k of Stage k will also serve as inputs for downstream stage $k+1$. Wen et al. developed a computer simulation for composite aircraft assembly process [6], [7], where the simulation needs multiple steps even for a single-stage assembly, as shown in Fig. 10. Therefore, the omnipresent nested structure needs to be incorporated when modeling computer experiments.

B. Literature Review

In this section, we conduct the literature review from three fields: mechatronics, advanced statistics, and manufacturing systems.

In the mechatronics field, Rodriguez et al. developed one hybrid control scheme with two nested loops for twisted string actuators [8]. Nested design techniques have been used for co-design of controlled systems [9]. Zeng et al. proposed a nested optimization strategy to guarantee cost control for a motor driving system [10]. The performance-based nested Kriging model was constructed to interpolate the Antenna characteristics data [11]. Nested long-short term memory (LSTM) networks were incorporated into deep learning architecture for multivariate air quality prediction [12]. A nested tensor product model transformation was used to analyze the Takagi-Sugeno fuzzy system for system control design [13]. These approaches make full use of the nested structure for various objectives (control, design, prediction, etc.) and achieve excellent performance.

In the advanced statistics field, researchers investigated nested effects in computer experiments. Nested space-filling designs were constructed for computer experiments with two levels of simulation accuracy [14]. Next, nested Latin hypercube designs with sliced structures were proposed for experimental data collection [15]. Hung et al. developed the optimal Latin hypercube designs and kriging methods incorporating nested factors and branching factors [16]. Marque-Pucheu et al. proposed an efficient dimension reduction method for Gaussian process emulation of two nested codes [17]. Keogh and White investigated nested case-control and case-cohort study on exposure-disease association [18]. These methods significantly improve the efficiency and effectiveness of data collection, model emulation, and association analysis in advanced statistics.

In the advanced manufacturing field, nested systems have also been investigated. Gibson et al. used multivariate nested distributions to model semiconductor process variability [19]. Similarly, Tian et al. analyzed the nested variation pattern in the batch processes of semiconductor manufacturing, and proposed a two-level nested control chart for process monitoring [20]. Jin and Shi developed a reconfigured piecewise linear regression tree to model the nested structure for process control in multistage manufacturing [21]. Savin and Vorochaeva developed a quadratic programming based controller with nested structure, and it achieved excellent performance in planar pipeline robots [22]. Wang et al. proposed multiresolution and multisensor fusion network for fault diagnosis, with integration of multiple network structures [23]. These methods enhanced variability modeling, process control, and quality assurance by accommodating the nested structure.

C. Novelty and Contributions

Although numerous techniques have been investigated in studying and using nested effect, as mentioned in the literature review above, global optimization for nested computer experiments still lacks a systematic science base. This paper focuses on the global optimization of nested computer experiments.

We mainly use *two-layer nested computer models* as one example for nested computer experiments. The first-layer code is denoted as the inner computer model, and the second one as the outer computer model. The nested structure indicates that the outputs of the inner computer model are part of inputs of the outer computer model. The inner computer model and outer computer model are very complex and they are assumed to be black-box.

Bayesian optimization is an efficient approach to obtain the global optimal solution for complex computer experiments given specific objectives. This approach has proven to be successful in various fields, such as materials design [24], hyperparameter tuning [25], advanced manufacturing [26]. The main steps of a standard Bayesian optimization method include: (i) Build a statistical surrogate model based on previous computer outputs; (ii) Choose an acquisition function and sequentially query the objective function at points which maximize the acquisition. For step (i), the most popular stochastic surrogate model is the Gaussian Process (GP) model [1]. For step (ii), commonly used acquisition functions include the Expected Improvement (EI) [27], the Lower/Upper Confidence Bound (LCB) [28], and the Expected Quantile Improvement (EQI) acquisition functions [29]. Despite the wide applications of Bayesian optimization methods, these existing methods ignored the outputs of the inner computer model and treated all the inputs characterizing the system of interest as a single input vector. When trying to find the global optimal solution of nested computer experiments, these existing Bayesian optimization methods are less efficient, since the nested structure information is ignored in the optimization. Astudillo and Frazier [30] considered Bayesian optimization of composite functions and took the outputs of the inner part of a composite function into account. This method performs excellent when the outer part of a composite function is a known, cheap-to-evaluated, and real-valued function. It does not work well for the complex black-box functions with nested structure, which is more common in engineering computer experiments.

In this work, we proposed a novel and systematic Bayesian optimization for nested computer experiments. We assume that both the inner and outer computer models are deterministic, but expensive-to-evaluate. Our contributions can be summarized as follows:

- The nested Bayesian optimization is proposed to incorporate the nested structures in complex computer experiments. This method can learn the global optimum more efficiently and avoid convergence to the local optimum.
- We investigated the theoretical properties given the nested Gaussian process is Gaussian or non-Gaussian. Furthermore, we derive the closed forms of nested expected improvement and propose a computational algorithm for nested Bayesian optimization.
- Based on the composite structures assembly case study, we show that nested Bayesian optimization can minimize the residual stress after assembly. We also show the proposed nested Bayesian optimization performs better than five benchmark methods via numerical studies.

The outline of this paper is as follows: Section II introduces the optimization problem of two-nested computer experiments. Section III proposes the nested Bayesian optimization method. Section IV and Section V compare the proposed method with the standard Bayesian optimization method by using three numerical studies and a real case study. Concluding remarks are given in Section VI. Appendices contain detailed proofs of the theorems and selection of correlation functions

II. PROBLEM SETTING

In this section, we use mathematical models to describe the problem setting. Denote $f : \mathcal{X} \rightarrow \mathbf{R}$ to be a nested computer model, which is defined as

$$f(\tilde{\mathbf{x}}) = g(\mathbf{h}^T(x), x'); \tilde{\mathbf{x}} = (x, x')^T \in \mathcal{X} \subset \mathbf{R}^d, \quad (1)$$

where $\mathbf{h}(x) = (h_1(x), \dots, h_p(x))^T$, $p \geq 1$ is a vector of inner computer model outputs. $g(\cdot)$ is the outer computer model whose inputs include outputs of the inner computer model $\mathbf{h}(x)$ and the additional control variable x' . Fig. 2 shows the framework of nested computer experiments:

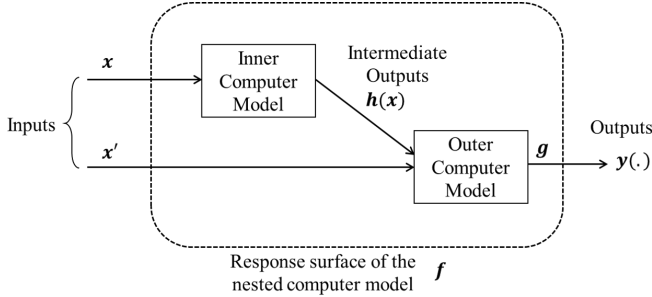


Fig. 2. Nested computer experiments.

Suppose these two computer models are black-box, deterministic, expensive-to-evaluate, and the gradient information is not available. With the help of a limited number of outputs from both computer models, we consider the problem of finding a minimizer of the entire response surface of the nested computer model f :

$$\tilde{\mathbf{x}}^* = \operatorname{argmin}_{\tilde{\mathbf{x}} \in \mathcal{X}} f(\tilde{\mathbf{x}}). \quad (2)$$

Specifically, suppose the nested computer experiments are conducted at the points $\tilde{X}_n = (\tilde{\mathbf{x}}_1, \dots, \tilde{\mathbf{x}}_n)^T$, which contains the collections of $\{\mathbf{x}_1, \dots, \mathbf{x}_n\}$ and $\{\tilde{\mathbf{x}}_1, \dots, \tilde{\mathbf{x}}_n\}$. The first-layer computer model generates intermediate outputs $H_n = (\mathbf{h}(x_1), \dots, \mathbf{h}(x_n))^T$, and the second-layer computer model generates the outputs $Y_n = (g(\mathbf{h}^T(x_1), x'_1), \dots, g(\mathbf{h}^T(x_n), x'_n))^T$. These computer experiments yield data $D_n = \{\tilde{X}_n, H_n, Y_n\}$. The goal of this work is to query $\tilde{\mathbf{x}}^*$ by making full use of the dataset D_n .

As discussed above, the standard Bayesian optimization method can be used to solve the optimization problem (2). This approach can query the optimal point of f sequentially by optimizing an acquisition function. In this work, we focus on the EI criterion [1], [27]. Detailed comparisons are conducted between EI, LCB, and EQI-based approaches in Section IV and Section V.

The main idea of EI is to sample the point offering the greatest expected improvement over the current best sampled point. Let $f_n^* = \min_{i=1}^n \{y_i\}$ be the current best objective value, given data $\{\tilde{X}_n, Y_n\}$, the EI function becomes:

$$\text{EI}_n(\tilde{\mathbf{x}}) = E_{f|\tilde{X}_n, Y_n} (f_n^* - f(\tilde{\mathbf{x}}))_+, \quad (3)$$

where $(f_n^* - f(\tilde{\mathbf{x}}))_+ = \max\{f_n^* - f(\tilde{\mathbf{x}}), 0\}$ is the improvement utility function.

It can be known that the evaluation of EI depends on the posterior distribution $f|\tilde{X}_n, Y_n$. Since the posterior distribution $f|\tilde{X}_n, Y_n$ in standard Bayesian optimization method ignores the outputs of the inner computer model, it leads to low optimization efficiency or even converges to the local optimum rather than the global optimum. To overcome this limitation, we will develop a new Bayesian optimization method to incorporate the nested structure and identify the optimal solution for complex computer experiments.

III. NESTED BAYESIAN OPTIMIZATION

In this section, we propose a novel method, named as *Nested Bayesian Optimization (NBO)*, to query the global optimal solution of nested computer experiments. To approximate the outputs of nested computer experiments, we first introduce nested Gaussian Process (NGP) models in Section III-A. Next, we derive the closed forms of the expected improvement acquisition function for nested computer experiments in Section III-B, under the cases that the NGP models are Gaussian and non-Gaussian. Section III-C provides a detailed algorithm of the NBO method.

A. Nested Gaussian Process models

In this work, Gaussian Process (GP) models [1] are used to mimic the inner and the outer computer models. Suppose h and g are realizations of two Gaussian Processes. Given data D_n , the posterior distribution of the inner computer model at an unobserved input x is

$$\mathbf{h}(x)|D_n \sim N(\hat{\mathbf{h}}_n(x), \mathbf{s}_h^2(x)), \quad (4)$$

where $\hat{\mathbf{h}}_n(x)$ is a $p \times 1$ mean vector, and $\mathbf{s}_h^2(x)$ is a $p \times p$ covariance matrix. The posterior distribution of the outer computer model at an unobserved input $x^{out} = (\mathbf{h}^T, x')$ is

$$g(x^{out})|D_n \sim N(\hat{g}_n(x^{out}), s_g^2(x^{out})). \quad (5)$$

Formulations of the posterior mean and posterior variance function are given by (22) and (23), respectively. More Details about the Gaussian Process models can be found in Appendix A.

The *nested Gaussian Process (NGP) model* is expressed as

$$f(\tilde{\mathbf{x}})|D_n = \hat{g}_n(\Psi^T(x), x') + s_g(\Psi^T(x), x')\xi_g. \quad (6)$$

where $\Psi(x) = \mathbf{h}(x)|D_n$, ξ_g is a standard normal random variable. From the posterior distribution of the inner computer model (4), $\Psi(x)$ can be represented as $\Psi(x) = \hat{\mathbf{h}}_n(x) + \mathbf{s}_h(x)\xi_h$, where ξ_h is a $p \times 1$ random vector that follows the normal distribution and it is independent from ξ_g . By numerical calculations, we have that, the posterior variance

of $f(\tilde{\mathbf{x}})|_{D_n}$ is zero for any $i = 1, \dots, n$, and the posterior mean is interpolating the observed data values (\tilde{X}_n, Y_n) .

It is worth noting that the nested Gaussian process may or may not be Gaussian [31]. Therefore, we will investigate two cases, Gaussian and non-Gaussian in the following part.

Taylor expansion of (6) shows that $f(\tilde{\mathbf{x}})|_{D_n}$ can be approximated by

$$Z(\tilde{\mathbf{x}}) = \mu_Z(\tilde{\mathbf{x}}) + \mathbf{c}_h^T(\tilde{\mathbf{x}})\boldsymbol{\xi}_h + c_g(\tilde{\mathbf{x}})\xi_g + \mathbf{c}_{h,g}^T(\tilde{\mathbf{x}})\boldsymbol{\xi}_h\xi_g, \quad (7)$$

where the global trend of $Z(\tilde{\mathbf{x}})$ is captured by $\mu_Z(\tilde{\mathbf{x}}) = \hat{g}_n(\hat{\mathbf{h}}_n^T(x), x')$. Uncertainty in $Z(\tilde{\mathbf{x}})$ due to the inner and outer GP models can be captured by $\mathbf{c}_h^T(\tilde{\mathbf{x}}) = \frac{\partial \hat{g}_n}{\partial \mathbf{h}}(\hat{\mathbf{h}}_n^T(x), x')\mathbf{s}_h(x)$ and $c_g(\tilde{\mathbf{x}}) = s_g(\hat{\mathbf{h}}_n^T(x), x')$, respectively. Uncertainty arising from the combined effect of the inner and outer models is measured by $\mathbf{c}_{h,g}^T(\tilde{\mathbf{x}}) = \frac{\partial s_g}{\partial \mathbf{h}}(\hat{\mathbf{h}}_n^T(x), x')\mathbf{s}_h(x)$. Provided that $Z(\tilde{\mathbf{x}})$ follows Gaussian or not, for a fixed $\tilde{\mathbf{x}} \in \mathcal{X}$, the distribution of $Z(\tilde{\mathbf{x}})$ is given in Theorem 1 and Theorem 2, respectively. Theorem 1 focuses on the Gaussian case, while Theorem 2 analyzes the non-Gaussian case.

Theorem 1: For a fixed $\tilde{\mathbf{x}} \in \mathcal{X}$, if $\mathbf{c}_{h,g}^T(\tilde{\mathbf{x}}) = \mathbf{0}_{1 \times p}$, $Z(\tilde{\mathbf{x}})$ is Gaussian:

$$Z(\tilde{\mathbf{x}}) \sim N(\mu_Z(\tilde{\mathbf{x}}), s_Z^2(\tilde{\mathbf{x}})) \quad (8)$$

where the variance function $s_Z^2(\tilde{\mathbf{x}})$ is $\mathbf{c}_h^T(\tilde{\mathbf{x}})\mathbf{c}_h(\tilde{\mathbf{x}}) + c_g^2(\tilde{\mathbf{x}})$.

Theorem 1 states the condition that $Z(\tilde{\mathbf{x}})$ to be a Gaussian random variable for a fixed $\tilde{\mathbf{x}}$. This result can be obtained by substituting the condition $\mathbf{c}_{h,g}^T(\tilde{\mathbf{x}}) = \mathbf{0}_{1 \times p}$ into (7).

The condition $\mathbf{c}_{h,g}^T(\tilde{\mathbf{x}}) = \frac{\partial s_g}{\partial \mathbf{h}}(\hat{\mathbf{h}}_n^T(x), x')\mathbf{s}_h(x) = \mathbf{0}_{1 \times p}$ is very strict. The reasons include:

- The k th element of $\frac{\partial s_g}{\partial \mathbf{h}}(\hat{\mathbf{h}}_n^T(x), x')$ equals to zero. It indicates that, variance of the outer GP predictor is insensitive to changes of h_k at $\hat{\mathbf{h}}_n(x)$, that is, $s_g(\hat{\mathbf{h}}_n^T(x) + \Delta \mathbf{h}^T, x') = s_g(\hat{\mathbf{h}}_n^T(x), x')$, where $\Delta \mathbf{h}$ is a $p \times 1$ vector whose elements are all 0 except for the k th element equals to $\Delta h_k > 0$. This condition may be challenging to achieve.
- $s_{h_k}(x)$ equals to zero. It indicates that the uncertainty of the GP predictor for h_k is zero. This condition is unattainable in some cases.

Since this condition is hard to achieve or even unattainable in some cases, we derive Lemma 1. Lemma 1 relaxes this condition and gives a necessary and sufficient condition for a NGP model (6) able to be approximated by a GP model.

Lemma 1: The NGP model (6) can be approximated by the following GP model

$$f(\tilde{\mathbf{x}})|_{D_n} \approx GP(\mu_Z(\tilde{\mathbf{x}}), s_Z^2(\tilde{\mathbf{x}})), \quad (9)$$

if and only if for all $\tilde{\mathbf{x}} \in \mathcal{X}$, there is $\mathbf{c}_{h,g}^T(\tilde{\mathbf{x}}) \approx \mathbf{0}_{1 \times p}$.

This result is derived from the relationship between normal random variables and a Gaussian Process [1].

Theorem 2: For a fixed $\tilde{\mathbf{x}} \in \mathcal{X}$, if $\mathbf{c}_{h,g}^T(\tilde{\mathbf{x}}) \neq \mathbf{0}_{1 \times p}$, $Z(\tilde{\mathbf{x}})$ is a non-Gaussian random variable. Let $Z_1(\tilde{\mathbf{x}})$ and $Z_2(\tilde{\mathbf{x}})$ are independent normal random variables with means $\mu_1(\tilde{\mathbf{x}}) = c_g(\tilde{\mathbf{x}})/\sqrt{\mathbf{c}_{h,g}^T(\tilde{\mathbf{x}})\mathbf{c}_{h,g}(\tilde{\mathbf{x}})}$, $\mu_2(\tilde{\mathbf{x}}) = \sqrt{\mathbf{c}_h^T(\tilde{\mathbf{x}})\mathbf{c}_h(\tilde{\mathbf{x}})}$ respectively and variances $\sigma_1^2(\tilde{\mathbf{x}}) = 1$, $\sigma_2^2(\tilde{\mathbf{x}}) = \mathbf{c}_{h,g}^T(\tilde{\mathbf{x}})\mathbf{c}_{h,g}(\tilde{\mathbf{x}})$ respectively. Let $z_0(\tilde{\mathbf{x}}) = \mu_Z(\tilde{\mathbf{x}}) - \mu_1(\tilde{\mathbf{x}})\mu_2(\tilde{\mathbf{x}})$. Then we have,

$$Z(\tilde{\mathbf{x}}) = Z_1(\tilde{\mathbf{x}})Z_2(\tilde{\mathbf{x}}) + z_0(\tilde{\mathbf{x}}). \quad (10)$$

The exact probability density function of $Z(\tilde{\mathbf{x}})$ is given by

$$p_Z(z) = \frac{\int_{-\infty}^{\infty} \frac{1}{|t|} \exp\left\{-\frac{u_1^2(t, \tilde{\mathbf{x}}) + u_2^2(z, t, \tilde{\mathbf{x}})}{2}\right\} dt}{2\pi\sigma_1(\tilde{\mathbf{x}})\sigma_2(\tilde{\mathbf{x}})}, \quad (11)$$

where $u_1(t, \tilde{\mathbf{x}}) = \frac{t - \mu_1(\tilde{\mathbf{x}})}{\sigma_1(\tilde{\mathbf{x}})}$, $u_2(z, t, \tilde{\mathbf{x}}) = \frac{z + z_0(\tilde{\mathbf{x}}) - t\mu_2(\tilde{\mathbf{x}})}{|t|\sigma_2(\tilde{\mathbf{x}})}$. The cumulative density function of $Z(\tilde{\mathbf{x}})$ is

$$P_Z(z) = \int_{-\infty}^{\infty} \phi_N(u_1(t, \tilde{\mathbf{x}}))\Phi_N(u_2(z, t, \tilde{\mathbf{x}}))dt, \quad (12)$$

where Φ_N is the cumulative distribution function of the standard normal distribution and ϕ_N is the probability density function. Mean and variance functions of $Z(\tilde{\mathbf{x}})$ are

$$\begin{aligned} E[Z(\tilde{\mathbf{x}})] &= \mu_Z(\tilde{\mathbf{x}}), \\ \text{Var}[Z(\tilde{\mathbf{x}})] &= \mathbf{c}_h^T(\tilde{\mathbf{x}})\mathbf{c}_h(\tilde{\mathbf{x}}) + c_g^2(\tilde{\mathbf{x}}) + \mathbf{c}_{h,g}^T(\tilde{\mathbf{x}})\mathbf{c}_{h,g}(\tilde{\mathbf{x}}). \end{aligned} \quad (13)$$

Detailed proofs of Theorem 2 are given in Appendix B.

Remark 1: If $z_0(\tilde{\mathbf{x}}) = 0$, $Z(\tilde{\mathbf{x}})$ follows a normal product (NP) distribution [32], which is in general non-Gaussian. Especially, if $Z_1(\tilde{\mathbf{x}}) \sim N(0, 1)$ and $Z_2(\tilde{\mathbf{x}}) \sim N(0, 1)$, then density function of $Z_1(\tilde{\mathbf{x}})Z_2(\tilde{\mathbf{x}})$ is

$$p_Z(z) = \frac{K_0(|z|)}{\pi}, \infty < z < +\infty.$$

Here K_0 denotes the modified Bessel function of the second kind with order 0. This density function exhibits a sharp peak at the origin and heavy tails.

Lemma 2: The NGP model (6) is a non-Gaussian Process model if and only if there is $\tilde{\mathbf{x}} \in \mathcal{X}$, such that $\mathbf{c}_{h,g}^T(\tilde{\mathbf{x}}) \neq \mathbf{0}_{1 \times p}$. Result of Lemma 2 is a direct conclusion of Theorem 2.

From Lemma 1 and 2, we have that, there is a great difference between the NGP and composite GP [33]. The composite GP model is an addition of two Gaussian Processes, where the first one captures the smooth global trend and the second one models local details. Thus the composite GP is still a Gaussian Process. However, the NGP may no longer be a Gaussian Process.

B. Closed forms of the Nested Expected Improvement (NEI)

To distinguish from the standard Bayesian optimization method, the EI function where NGP is used to approximate the nested computer experiments is called *Nested Expected Improvement (NEI)* function:

$$\text{NEI}_n(\tilde{\mathbf{x}}) = E_{f|D_n}(f_n^* - f(\tilde{\mathbf{x}}))_+, \quad (14)$$

A new queried point $\tilde{\mathbf{x}}_{n+1}$ is selected by maximizing the $\text{NEI}_n(\tilde{\mathbf{x}})$ function

$$\tilde{\mathbf{x}}_{n+1} = \underset{\tilde{\mathbf{x}} \in \mathcal{X}}{\text{argmax}} \text{NEI}_n(\tilde{\mathbf{x}}). \quad (15)$$

We can see that values of NEI_n depend on the posterior distribution $f(\tilde{\mathbf{x}})|_{D_n}$. Given two cases depending on whether NGP model can be approximated by a Gaussian process, the NEI acquisition function also has different expressions. We will investigate NEI function in the following two theorems.

Theorem 3: If the NGP model can be approximated by the GP model (9), denote $v(\tilde{\mathbf{x}}) = \frac{f_n^* - \mu_Z(\tilde{\mathbf{x}})}{s_Z(\tilde{\mathbf{x}})}$, the NEI acquisition function has the closed-form expression:

$$(f_n^* - \mu_Z(\tilde{\mathbf{x}}))\Phi_N(v(\tilde{\mathbf{x}})) + s_Z(\tilde{\mathbf{x}})\phi_N(v(\tilde{\mathbf{x}})). \quad (16)$$

A detailed proof of this theorem can be found in [27]. The NEI acquisition function (16) implicitly encodes a tradeoff between exploration of the feasible region and exploitation near the current best solution. The first term in (16) encourages exploitation, by assigning larger values for points with smaller predicted values; the second term in (16) encourages exploration, by assigning greater values for points with larger estimated posterior variance.

Theorem 4: If the NGP model can't be approximated by a GP model, the NEI acquisition function can be evaluated by:

$$\int_{-\infty}^{\infty} (f_n^* - z_0(\tilde{\mathbf{x}}) - t\mu_2(\tilde{\mathbf{x}}))\phi_N(u_1(t, \tilde{\mathbf{x}}))\Phi_N(u_2(f_n^*, t, \tilde{\mathbf{x}})) + |t|\sigma_2(\tilde{\mathbf{x}})\phi_N(u_1(t, \tilde{\mathbf{x}}))\phi_N(u_2(f_n^*, t, \tilde{\mathbf{x}})) dt. \quad (17)$$

Detailed proofs of this theorem can be found in Appendix B. Markov Chain Monte Carlo (MCMC) method can be used to estimate NEI_n (17). Because $\phi_N(u_1(t, \tilde{\mathbf{x}})) = 0$ as $u_1(t, \tilde{\mathbf{x}})$ tends to infinity, the interval of integration $t \in (-\infty, \infty)$ can be shrunk to $t \in [L_t(\tilde{\mathbf{x}}), U_t(\tilde{\mathbf{x}})]$, where $L_t(\tilde{\mathbf{x}})$ and $U_t(\tilde{\mathbf{x}})$ are pre-specified, such as $L_t = -10\sigma_1(\tilde{\mathbf{x}}) + \mu_1(\tilde{\mathbf{x}})$ and $U_t = 10\sigma_1(\tilde{\mathbf{x}}) + \mu_1(\tilde{\mathbf{x}})$ respectively.

Remark 2: Sampled Expected Improvement (SEI) as suggested in [34] is a commonly used method to estimate EI values when $f(\tilde{\mathbf{x}}|D_n)$ is non-Gaussian. SEI estimates EI values based on a large number of posterior samples of $f(\tilde{\mathbf{x}}|D_n)$ and only the prediction posterior samples that are smaller than the current best value are taken in the calculation. Since generating posterior samples of $f(\tilde{\mathbf{x}}|D_n)$ by using the posterior density function (11) is rather time-consuming, this method loses attraction.

C. Algorithm

In this subsection, we develop the computational algorithm for nested Bayesian optimization. Algorithm 1 provides detailed steps of the NBO method.

We can explain this algorithm as follows. Firstly, initial data is collected based on a maximin Latin hypercube design. Here, the number of initial points n_0 is set at $10d$, as recommended in [35]. Next, Gaussian Process models are built to mimic the inner model and the outer model by using (4) and (5). Then, K -fold cross-validation method is used to exam whether the NGP is a GP or not. More specifically, build GP model (8) to approximate the nested computer outputs and then examine the prediction accuracy of this GP model by K -fold cross-validation method. Here, choice of K follows the criterion below [36]

$$K \approx \log(n) \text{ and } n/K > 3d.$$

Finally, query the sequential points by maximizing (16) (when NGP is Gaussian) or by maximizing (17) (when NGP is non-Gaussian), until the sample size budget N is reached.

IV. NUMERICAL STUDIES

In this section, we compare the proposed NEI method with five benchmark methods. The five benchmark methods include (1) EI-GP: the Expected Improvement (EI) method under the one-GP model; (2) LCB-GP: the Lower Confidence Bound (LCB) method under the one-GP model; (3) LCB-NGP:

Algorithm 1 Nested Bayesian optimization

- 1: Obtain an initial design \tilde{X}_{n_0} with n_0 points, and run the nested computer models at these points, yielding corresponding simulator outputs H_{n_0}, Y_{n_0} .
 - 2: **for** iteration $n = n_0, \dots, N - 1$ **do**
 - 3: Evaluate the current best optimal point $\tilde{\mathbf{x}}_n^* = \operatorname{argmin} Y_n$ and the corresponding function value $f_n^* = \min Y_n$.
 - 4: Build GP models (4) and (5) to mimic the inner and the outer computer models respectively.
 - 5: Test whether the NGP model is a GP model by using a cross-validation method.
 - 6: **if** NGP model is Gaussian **then**
 - 7: Identify the maximizer $\tilde{\mathbf{x}}_{n+1}$ of NEI_n (16).
 - 8: **else**
 - 9: Identify the maximizer $\tilde{\mathbf{x}}_{n+1}$ of NEI_n (17).
 - 10: **end if**
 - 11: Run the nested computer models at $\tilde{\mathbf{x}}_{n+1}$, augment \tilde{X}_n, H_n and Y_n with $\tilde{\mathbf{x}}_{n+1}, h(x_{n+1})$ and $f(\tilde{\mathbf{x}}_{n+1})$.
 - 12: **end for**
 - 13: **Return** the current best optimal point $\tilde{\mathbf{x}}_N^* = \operatorname{argmin} Y_N$ and the corresponding function value $f_N^* = \min Y_N$.
-

the Lower Confidence Bound (LCB) method under the NGP model with default tuning parameter 2.96 as recommended in [37]; (4) EQI-GP: the Expected Quantile Improvement (EQI) method under the one-GP model; and (5) EQI-NGP: the Expected Quantile Improvement (EQI) method under the NGP model.

The simulation set-up is as follows. We generate the inputs \tilde{X}_{n_0} , where $n_0 = 10d$, according to a maximin Latin hypercube design via the R package *maximinLHS*. Then, we collect the inner computer model outputs H_{n_0} , and the outer computer model outputs Y_{n_0} on H_{n_0} and \tilde{X}_{n_0} .

To obtain the NGP predictor, two GP models are built to mimic the inner and outer computer models, respectively. Here, the GP models are fitted using the R package *DiceKriging* [38].

The log-optimality gap is used to compare the performance of different methods, which is defined as

$$\log_{10}(f_n^* - f^*).$$

All results about the log-optimality gap are averaged over 50 replications.

A. 1-d GP model

Suppose the inner computer model and the outer computer model are both commonly used one-dimension test functions in the literature on GP models [1]:

$$h(x) = \exp(-1.4x) \cos(7\pi x/2) - 1.4x, x \in [0, 1], \\ g(h) = h \sin(\pi h/2).$$

The global minimum of $f(x) = g(h(x))$ is at $x^* = 0.124$ and the corresponding function value is 0.

By choosing Matérn correlation functions (20) with smoothness parameter $\nu = 3/2$ as correlation functions, two GP

models are built to mimic the inner and outer computer models, respectively. To illustrate the results we choose Matérn correlation functions, a detailed comparison of the model accuracy between the one-GP model and the NGP model under different correlation functions is given in Appendix C. Fig. 3 shows predictors and 95% confidence intervals given by these two GP models.

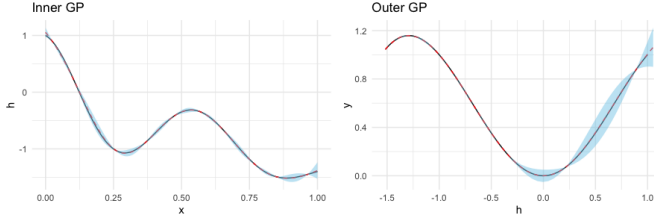


Fig. 3. The true inner and outer computer models (black real lines) v.s. GP predictions (red dotted lines) and 95% confidence intervals (blue intervals) of the inner computer model (left) and outer computer model (right).

From Fig. 3, we can find that the inner and outer computer models can be approximated by GP models perfectly. Moreover, 95% confidence intervals of the inner GP predictor show that $s_h(x)$ is almost zero for all $x \in [0, 1]$. Therefore, $f(\tilde{x})$ can be approximated by a GP model. To further verify this conclusion, a Gaussianity test is then conducted.

By the 3-fold cross-validation (CV) method, we have that, the NGP model is a GP model. Fig. 4 compares the performance of the one-GP build by using $(\tilde{X}_{n_0}, Y_{n_0})$ and the NGP model approximated by a composite GP model. It can be seen that, both mean functions of the one-GP model and the NGP model match the true function accurately, but the 95% confidence intervals indicate that, the NGP predictor has smaller variance than the one-GP predictor.

The reason for this result is that, f is a realization from a non-stationary GP. Compared to the stationary one-GP model, the NGP model can approximate f more accurately and can also improve the prediction intervals, especially when the experimental design is sparse [33].

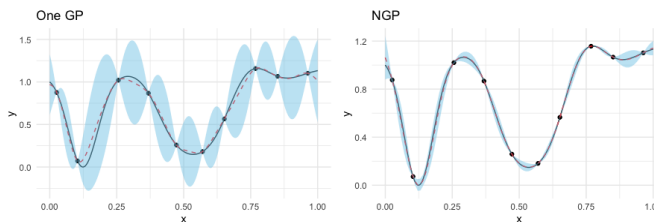


Fig. 4. Left: predictions (red dotted line) and 95% confidence intervals of the one-GP model build by using $(\tilde{X}_{n_0}, Y_{n_0})$, with $n_0 = 10$; Right: predictions (red dotted line) and 95% confidence intervals of the NGP model.

Fig. 5 shows the log-optimality gap against the number of samples for the six methods.

From Fig. 5, we can see that, the optimality gaps for NEI, LCB-NGP and LCB-GP enjoy steady improvements as n increases, whereas the optimality gap for the other methods stagnates for larger sample sizes. The proposed method and the LCB-NGP method outperform other methods. The NGP-based approaches outperform the one GP-based approaches

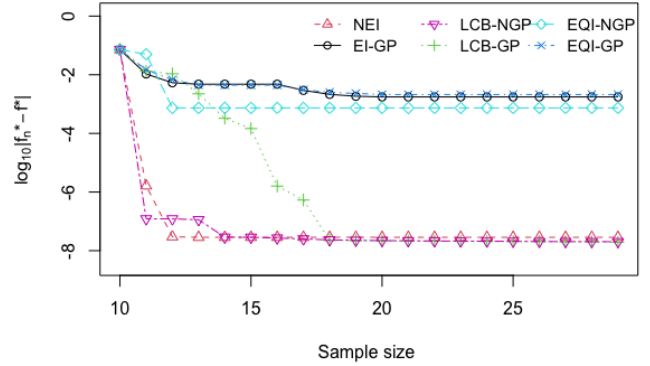


Fig. 5. Average optimality gap over 50 replications by different methods.

under the same acquisition function. This is a very direct result of the more accurate predictions for the NGP model.

B. 1-d non-GP model

Suppose the inner computer model is

$$h(x) = (1 + |x|)^{-4}, x \in [-1, 1],$$

and the outer computer model is

$$g(h) = h \sin(7\pi h/2).$$

The global minimum of this nested computer experiment is $(0, -1)$. Fig. 6 compares the performance of one GP model and NGP model with $n_0 = 10$.

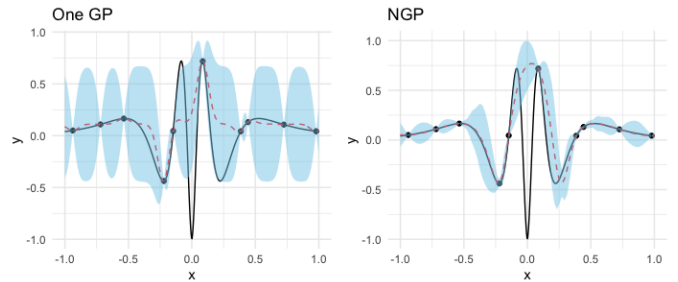


Fig. 6. Left: predictions (red dotted line) and 95% confidence intervals of the one-GP model build by using $(\tilde{X}_{n_0}, Y_{n_0})$, with $n_0 = 10$; Right: predictions (red dotted line) and 95% confidence intervals of the NGP model.

Fig. 6 shows that both the one-GP model and the NGP model perform poor in $x \in [-0.1, 0.1]$. The reason is that, values of the true function change fast in $x \in [-0.1, 0.1]$, but the design is sparse in $[-0.1, 0.1]$. Except at the points that belong to $[-0.1, 0.1]$, the NGP model outperforms the one-GP model.

Via the 3-fold CV test, we can find that the NGP model is not Gaussian. Therefore, in the NBO algorithm, the sequential point is collected by maximizing NEI_n (17). Set $L_t = -10\sigma_1(x) + \mu_1(x)$ and $U_t = 10\sigma_1(x) + \mu_1(x)$, MCMC method is used to evaluate (17) and the EQI function. The

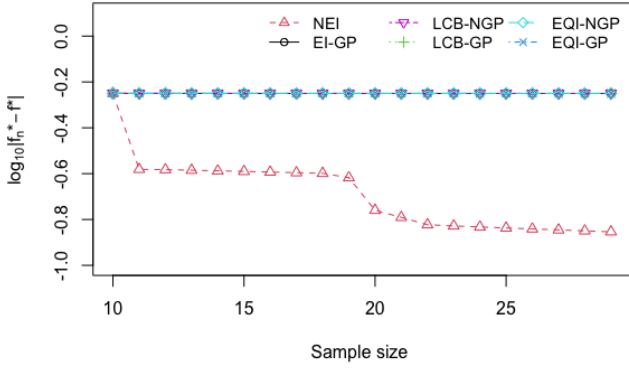


Fig. 7. Average optimality gap over 50 replications by different methods.

log-optimality gaps against the number of samples for the six methods are shown in Fig. 7.

From Fig. 7, we can conclude that the proposed method obtains a nearly optimum as n increases. However, the other methods fall into a local optimal point, which is included in the initial design. This shows that only the proposed method balances the optimal point of the fitted model with the exploration of other regions.

It is worth noting that, since the LCB depends only on the posterior mean and variance of $f(\tilde{\mathbf{x}})$, this acquisition function lose its advantage when the posterior distribution of $f(\tilde{\mathbf{x}})$ is non-Gaussian.

C. 4-d GP model

Suppose the inner computer model includes two functions: the three-hump camel function

$$h_1(\mathbf{x}) = 2x_1^2 - 1.05x_1^4 + x_1^6/6 + x_1x_2 + x_2^2,$$

and the six-hump camel function

$$h_2(\mathbf{x}) = (4 - 2.1x_3^2 + x_3^4/3)x_3^2 + x_3x_4 + (-4 + 4x_4^2)x_4^2,$$

Here, $\mathbf{x} = (x_1, x_2, x_3, x_4) \in [-1, 1]^4$. Suppose the outer computer model is the Branin function

$$g(\mathbf{h}) = \frac{1}{51.95} \left[g_1(\mathbf{h}) + \left(10 - \frac{10}{8\pi}\right) \cos(\bar{h}_1) - 44.81 \right],$$

where $g_1(\mathbf{h}) = (\bar{h}_2 - \frac{5.1\bar{h}_1^2}{4\pi^2} + \frac{5\bar{h}_1}{\pi} - 6)^2$, $\bar{h}_1 = 5(h_1 - 1)$, $\bar{h}_2 = 5(h_2 + 1)$. The global minimum of $f = g(\mathbf{h}(\mathbf{x}))$ is at $\mathbf{x}^* = (-0.121, 0.547, 0.915, 0.715)$ and the corresponding function value is -16.644 . Let $n_0 = 40$, we still use the maximin Latin hypercube design to collect data. Then we build GP models for inner and outer computer models. Via the 3-fold CV test, we have that the NGP model is Gaussian.

Fig. 8 compares the prediction performance of one GP model and NGP model at 100 un-observed locations. These 100 testing locations are sampled by the maximin Latin hypercube design. Left of Fig. 8 shows the comparison between

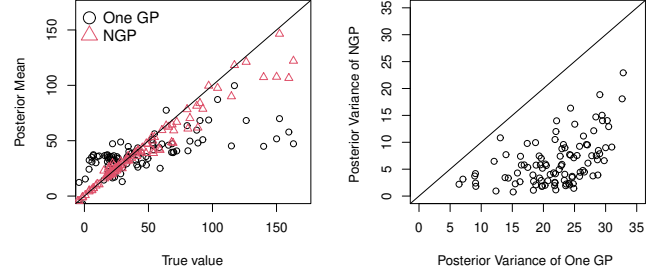


Fig. 8. Left: Posterior mean of the one-GP (black circles) and NGP (red triangles); Right: Posterior variance of the one-GP and NGP.

predictions of different models and the true outputs of the nested computer experiment. We see that, predictions given by the NGP model at these testing locations are much closer to the true values. The 100 points (black circles) in Fig. 8 right compare the posterior variances given by the one-GP model and the NGP model. Because all 100 points are under the line “ $y = x$ ”, it indicates that posterior variances given by the NGP model are smaller than posterior variances given by the one-GP model.

Fig. 9 shows the log-optimality gap $\log_{10}(f_n^* - f^*)$ against the number of samples n . Results of the log-optimality gap are averaged over 50 replications.

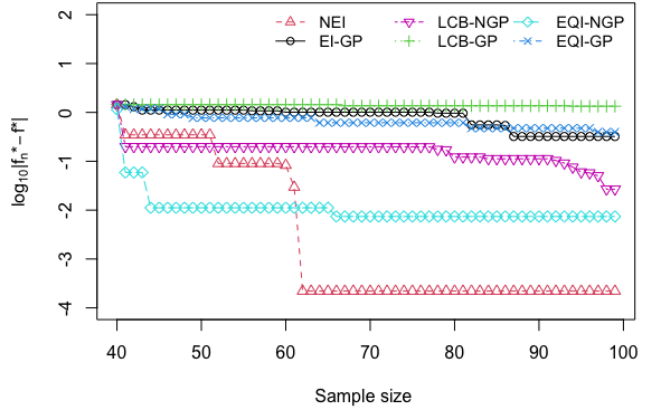


Fig. 9. Average optimality gap over 50 replications by different methods.

We can see from Fig. 9 that the proposed method outperforms other methods: the optimality gap for the latter methods stagnates for larger sample sizes, whereas the former enjoys steady improvements as n increases.

In summary, results of the numerical simulations show that the proposed NBO method has three advantages: (i) it incorporates the nested structure information and makes full use of the inner computer model outputs; (ii) it improves the prediction accuracy significantly; (iii) it avoids the convergence to local minimum and identifies the global optimum more efficiently.

V. CASE STUDY VIA COMPOSITE STRUCTURES ASSEMBLY

Composite structures have become increasingly used in many major products (e.g., fuselages, wings, car bodies, solar panels, spacecraft) due to their superior characteristics including high strength-to-weight ratio, high stiffness-to-weight ratio, potential long life, and low life-cycle cost. However, fabrication deviations are inevitable in composite structures. It is timely important to address the quality control in composite structures assembly.

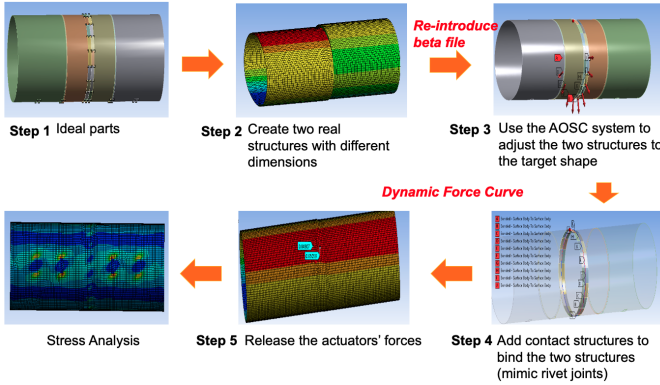


Fig. 10. The computer experiment mimics the composite structures assembly process.

One digital twin simulation platform for composite structures assembly was developed to mimic the fabrication process of carbon-fiber reinforced composites [6], [7]. This computer simulation platform was built based on ANSYS PrepPost Composites workbench, and it was calibrated and validated via physical experiments. The calibration process refers to [39]. The digital twin simulation can conduct virtual assembly to illustrate detailed composite structures joint. As shown in Fig. 10, the virtual assembly simulation includes multiple steps: (i) generate composite structures with deviations, (ii) apply Automatic Optimal Shape Control technique [40] to adjust the dimensions; (iii) add rivet joints and then release actuators' forces; (iv) do dimensional analysis and stress analysis.

This multistep computer simulation for composite structure assembly has nested structure. As shown in Fig. 11, the inner computer model simulates the shape control of a single composite structure. The automatic optimal shape control can adjust the dimensional deviations of one composite fuselage and make it align well with the other fuselage to be assembled. The outer computer model simulates the process of composite structures assembly, where the inputs are critical dimensions from two parts, and the outputs are internal stress after assembly. Table I summarizes the inputs and outputs information in computer experiments. We will conduct nested Bayesian optimization for this nested computer experiment to identify the optimal assembly that can minimize the residual stress after assembly.

Let $n_0 = 100$, we collect the inner computer model outputs H_{n_0} on a maximin Latin hypercube design X_{n_0} , and the outer computer model outputs Y_{n_0} on (H_{n_0}, X_{n_0}) . We conduct the 2-fold CV test and find that the NGP model is non-Gaussian. We split the initial data into 70% as training and 30% as a

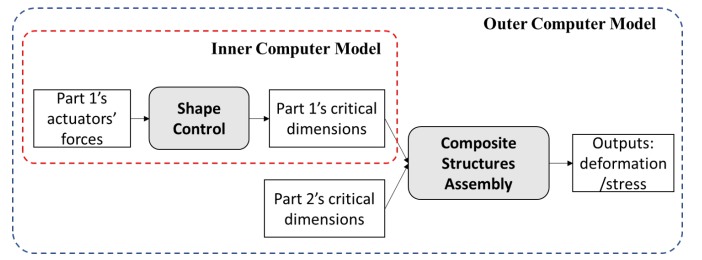


Fig. 11. Nested computer experiments in composite structures assembly.

testing set randomly, and use the training data to build the GP and NGP models. The testing data is used to compare the prediction accuracy of different models.

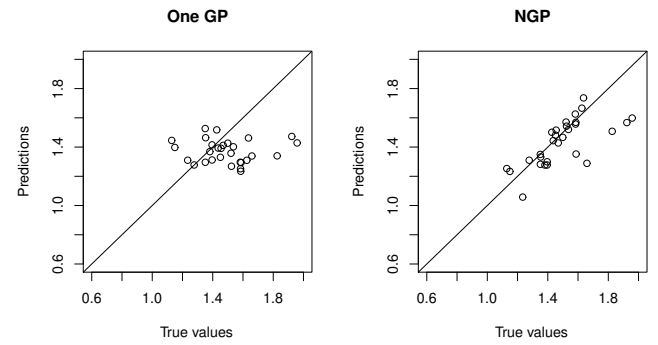


Fig. 12. Predictions given by the GP (left) and NGP (right) v.s. the true outputs.

Fig. 12 shows that the NGP model outperforms the one-GP model. Because the dimension of the inputs is 15, it is time-consuming to search the optimal point of EI and NEI function in Bayesian optimization. Following [41], instead of directly optimize the acquisition functions over \mathcal{X} , we choose a set of candidate point \mathcal{X}_{cand} from the whole search domain and then find the next point in \mathcal{X}_{cand} . In this work, we select \mathcal{X}_{cand} on a maximin Latin hypercube design and the sample size of \mathcal{X}_{cand} is set to be 1000. Let $N = 200$, Fig.13 shows the optimal results given by different methods. From Fig.13,

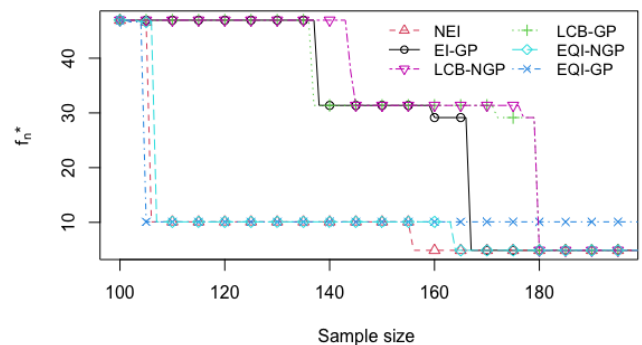


Fig. 13. The optimal results given by different methods.

TABLE I
INPUTS AND OUTPUTS FOR THE NESTED COMPUTER EXPERIMENTS

Inner computer model			
Inputs	Part 1's actuators' forces ($\tilde{\mathbf{x}}_1$)	$d = 10$	$\tilde{\mathbf{x}}_{1i} \in (-250, 250)$
Outputs	Part 1's critical dimensions ($\mathbf{h}(\tilde{\mathbf{x}}_1)$)	$d = 5$	
Outer computer model			
Inputs	Part 1's critical dimensions ($\mathbf{h}(\tilde{\mathbf{x}}_1)$)	$d = 5; (V_4, V_{16}, V_{28}, V_{40}, V_{52})$	
	Part 2's critical dimensions ($\tilde{\mathbf{x}}_2$)	$d = 5; (V_4, V_{16}, V_{28}, V_{40}, V_{52})$	
Outputs	Mean of Stress	$d = 1$	
Inputs			

we have that except for the EQI method under one-GP model, the others obtain the same minimum of residual stress with 4.885 psi (pound per square inch). Moreover, the proposed method identifies this residual stress with a minimum number of sequential points, which indicates the high effectiveness of the proposed method.

VI. SUMMARY AND DISCUSSIONS

Computer experiments and digital twins have ubiquitous influence on engineering systems. Since the multi-step simulations or hierarchical structure of systems, many computer experiments have nested structures. This paper proposed a novel Bayesian optimization for nested computer experiments. We first derived the nested Gaussian process models to serve as surrogates for the computer models. We proved the distribution of nested outputs given it is Gaussian or non-Gaussian. We also deduced the closed forms of nested expected improvement, and proposed one new algorithm for nested Bayesian optimization. The proposed NBO method can make full use of the nested structure and intermediate outputs to identify the global optimum efficiently. It avoids convergence to the local optimum which may occur in standard Bayesian optimization. We validated the performance of NBO based on three numerical studies and one case study. In the case study, the proposed NBO can minimize the residual stress for composite structures assembly, and achieve a much better result than the conventional Bayesian optimization.

The proposed method may be faced with generalizability challenge when the system has multiple connected models. Specifically, approximating the multiple nested computer models by a suitable surrogate model needs to estimate more hyperparameters. More training samples will be required for accurate parameter learning. High-dimensionality of parameters may result in high computational cost of Bayesian optimization. Furthermore, the fitting multiple connected computer models by a nested GP may have non-identifiability issue. In future research, we will investigate the identifiability conditions and new nested Bayesian optimization for complex multiple connected systems.

ACKNOWLEDGMENT

Dr. Wang's research was supported by the National Natural Science Foundation of China (12101024), the Natural Science Foundation of Beijing Municipality (1214019).

REFERENCES

- [1] T. J. Santner, B. J. Williams, and W. I. Notz, *The design and analysis of computer experiments (Ed 2)*. Springer Science & Business Media, 2018, vol. 1.
- [2] J. Shi, *Stream of variation modeling and analysis for multistage manufacturing processes*. CRC press, 2006.
- [3] S. Zhou, Q. Huang, and J. Shi, "State space modeling of dimensional variation propagation in multistage machining process using differential motion vectors," *IEEE Transactions on Robotics and Automation*, vol. 19, no. 2, pp. 296–309, 2003.
- [4] J. Jin and J. Shi, "State space modeling of sheet metal assembly for dimensional control," *ASME Transactions, Journal of Manufacturing Science and Engineering*, vol. 121, no. 4, pp. 756–762, 1999.
- [5] T. Zhang and J. Shi, "Stream of variation modeling and analysis for compliant composite part assembly—part ii: Multistation processes," *Journal of Manufacturing Science and Engineering*, vol. 138, no. 12, 2016.
- [6] Y. Wen, X. Yue, J. H. Hunt, and J. Shi, "Feasibility analysis of composite fuselage shape control via finite element analysis," *Journal of Manufacturing Systems*, vol. 46, pp. 272–281, 2018.
- [7] —, "Virtual assembly and residual stress analysis for the composite fuselage assembly process," *Journal of Manufacturing Systems*, vol. 52, pp. 55–62, 2019.
- [8] A. S.-M. Rodriguez, M. Hosseini, and J. Paik, "A hybrid control strategy for force and precise end effector positioning of a twisted string actuator," *IEEE/ASME Transactions on Mechatronics*, 2020.
- [9] A. Kamadan, G. Kiziltas, and V. Patoglu, "Co-design strategies for optimal variable stiffness actuation," *IEEE/ASME Transactions on Mechatronics*, vol. 22, no. 6, pp. 2768–2779, 2017.
- [10] T. Zeng, X. Ren, Y. Zhang, G. Li, and J. Na, "An integrated optimal design for guaranteed cost control of motor driving system with uncertainty," *IEEE/ASME Transactions on Mechatronics*, vol. 24, no. 6, pp. 2606–2615, 2019.
- [11] S. Koziel and A. Pietrenko-Dabrowska, "Performance-based nested surrogate modeling of antenna input characteristics," *IEEE Transactions on Antennas and Propagation*, vol. 67, no. 5, pp. 2904–2912, 2019.
- [12] N. Jin, Y. Zeng, K. Yan, and Z. Ji, "Multivariate air quality forecasting with nested lstm neural network," *IEEE Transactions on Industrial Informatics*, 2021.
- [13] Y. Yu, Z. Li, X. Liu, K. Hirota, X. Chen, T. Fernando, and H. H. Iu, "A nested tensor product model transformation," *IEEE Transactions on Fuzzy Systems*, vol. 27, no. 1, pp. 1–15, 2018.
- [14] P. Z. Qian, B. Tang, and C. J. Wu, "Nested space-filling designs for computer experiments with two levels of accuracy," *Statistica Sinica*, pp. 287–300, 2009.
- [15] H. Chen and M.-Q. Liu, "Nested latin hypercube designs with sliced structures," *Communications in Statistics-Theory and Methods*, vol. 44, no. 22, pp. 4721–4733, 2015.
- [16] Y. Hung, V. R. Joseph, and S. N. Melkote, "Design and analysis of computer experiments with branching and nested factors," *Technometrics*, vol. 51, no. 4, pp. 354–365, 2009.
- [17] S. Marque-Pucheu, G. Perrin, and J. Garnier, "An efficient dimension reduction for the gaussian process emulation of two nested codes with functional outputs," *Computational Statistics*, vol. 35, no. 3, pp. 1059–1099, 2020.
- [18] R. H. Keogh and I. R. White, "Using full-cohort data in nested case-control and case-cohort studies by multiple imputation," *Statistics in Medicine*, vol. 32, no. 23, pp. 4021–4043, 2013.
- [19] D. S. Gibson, R. Poddar, G. S. May, and M. A. Brooke, "Using multivariate nested distributions to model semiconductor manufacturing processes," *IEEE Transactions on Semiconductor Manufacturing*, vol. 12, no. 1, pp. 53–65, 1999.
- [20] W. Tian, H. You, K. Gu, C. Zhang, and X. Jia, "Two-level nested control chart for batch process in the semiconductor manufacturing," *IEEE Transactions on Semiconductor Manufacturing*, vol. 29, no. 4, pp. 399–410, 2016.
- [21] R. Jin and J. Shi, "Reconfigured piecewise linear regression tree for multistage manufacturing process control," *IIE Transactions*, vol. 44, no. 4, pp. 249–261, 2012.

- [22] S. Savin and L. Vorochaeva, "Nested quadratic programming-based controller for pipeline robots," in *2017 International Conference on Industrial Engineering, Applications and Manufacturing (ICIEAM)*. IEEE, 2017, pp. 1–6.
- [23] J. Wang, P. Fu, L. Zhang, R. X. Gao, and R. Zhao, "Multilevel information fusion for induction motor fault diagnosis," *IEEE/ASME Transactions on Mechatronics*, vol. 24, no. 5, pp. 2139–2150, 2019.
- [24] Y. Zhang, D. W. Apley, and W. Chen, "Bayesian optimization for materials design with mixed quantitative and qualitative variables," *Scientific Reports*, vol. 10, no. 1, pp. 1–13, 2020.
- [25] F. Archetti and A. Candelieri, *Bayesian optimization and data science*. Springer, 2019.
- [26] X. Guidetti, A. Rupenyan, L. Fassi, M. Nabavi, and J. Lygeros, "Sample-efficient plasma spray process configuration with constrained bayesian optimization," *arXiv preprint arXiv:2103.13881*, 2021.
- [27] D. R. Jones, M. Schonlau, and W. J. Welch, "Efficient global optimization of expensive black-box functions," *Journal of Global Optimization*, vol. 13, no. 4, pp. 455–492, 1998.
- [28] N. Srinivas, A. Krause, S. Kakade, and M. Seeger, "Gaussian process optimization in the bandit setting: No regret and experimental design," in *Proceedings of the 27th International Conference on Machine Learning*, no. CONF. Omnipress, 2010.
- [29] V. Picheny, D. Ginsbourger, Y. Richet, and G. Caplin, "Quantile-based optimization of noisy computer experiments with tunable precision," *Technometrics*, vol. 55, no. 1, pp. 2–13, 2013.
- [30] R. Astudillo and P. I. Frazier, "Bayesian optimization of composite functions," *arXiv preprint arXiv:1906.01537*, 2019.
- [31] S. Marque-Pucheu, G. Perrin, and J. Garnier, "Efficient sequential experimental design for surrogate modeling of nested codes," *ESAIM: Probability and Statistics*, vol. 23, pp. 245–270, 2019.
- [32] G. Cui, X. Yu, S. Iommelli, and L. Kong, "Exact distribution for the product of two correlated gaussian random variables," *IEEE Signal Processing Letters*, vol. 23, no. 11, pp. 1662–1666, 2016.
- [33] S. Ba, V. R. Joseph *et al.*, "Composite gaussian process models for emulating expensive functions," *The Annals of Applied Statistics*, vol. 6, no. 4, pp. 1838–1860, 2012.
- [34] R.-B. Chen, Y. Wang, and C. J. Wu, "Finding optimal points for expensive functions using adaptive rbf-based surrogate model via uncertainty quantification," *Journal of Global Optimization*, pp. 1–30, 2020.
- [35] J. L. Loepky and S. W. J. Welch, "Special issue on computer modeling — choosing the sample size of a computer experiment: A practical guide," *Technometrics*, vol. 51, no. 4, pp. 366–376, 2009.
- [36] Y. Jung, "Multiple predicting k-fold cross-validation for model selection," *Journal of Nonparametric Statistics*, vol. 30, no. 1, pp. 197–215, 2018.
- [37] Z. Chen, S. Mak, and C. Wu, "A hierarchical expected improvement method for bayesian optimization," *arXiv preprint arXiv:1911.07285*, 2019.
- [38] O. Roustant, D. Ginsbourger, Y. D. Contributors, and M. O. Roustant, "Package 'dicekriging'," 2015.
- [39] Y. Wang, X. Yue, R. Tuo, J. H. Hunt, J. Shi *et al.*, "Effective model calibration via sensible variable identification and adjustment with application to composite fuselage simulation," *Annals of Applied Statistics*, vol. 14, no. 4, pp. 1759–1776, 2020.
- [40] X. Yue, Y. Wen, J. H. Hunt, and J. Shi, "Surrogate model-based control considering uncertainties for composite fuselage assembly," *Journal of Manufacturing Science and Engineering*, vol. 140, no. 4, 2018.
- [41] R.-B. Chen, Y. Wang, and C. F. J. Wu, "Finding optimal points for expensive functions using adaptive rbf-based surrogate model via uncertainty quantification," *Journal of Global Optimization*, vol. 77, no. 4, pp. 919–948, 2020.

APPENDIX A GAUSSIAN PROCESS MODELS

In this section, we introduce GP models to mimic the inner and outer computer outputs. Suppose

$$\begin{aligned} h_k(\cdot) &= \mu_{h_k}(\cdot) + Z_{h_k}(\cdot), k = 1, \dots, p, \\ \mu_{h_k}(\cdot) &= \mathbf{b}_{h_k}^T(\cdot)\boldsymbol{\beta}_{h_k}, Z_{h_k}(\cdot) \sim GP(\mathbf{0}, \sigma_{h_k}^2 \Phi_{h_k}); \\ g(\cdot) &= \mu_g(\cdot) + Z_g(\cdot), \\ \mu_g(\cdot) &= \mathbf{b}_g^T(\cdot)\boldsymbol{\beta}_g, Z_g(\cdot) \sim GP(0, \sigma_g^2 \Phi_g). \end{aligned} \quad (18)$$

For the k 'th output of inner computer model, $\mathbf{b}_{h_k}(\cdot)$ consists of q_{h_k} basis functions for the mean function μ_{h_k} ; $\boldsymbol{\beta}_{h_k}$ denotes its corresponding coefficients, and $GP(0, \sigma_{h_k}^2 \Phi_{h_k})$ denotes a stationary Gaussian Process with mean zero, variance $\sigma_{h_k}^2$ and correlation function $\Phi_{h_k}(\cdot)$. For the outer computer model, $g(\cdot) \sim GP(\mathbf{b}_g^T(\cdot)\boldsymbol{\beta}_g, \sigma_g^2 \Phi_g)$, where \mathbf{b}_g and $\boldsymbol{\beta}_g$ are $q_g \times 1$ vectors; σ_g^2 is the process variance and $\Phi_g(\cdot)$ is the correlation function. Common choices of $\Phi_{h_k}(\tilde{h})$ and $\Phi_g(\tilde{h})$ include the Gaussian correlation functions

$$\exp(-\theta \tilde{h}^2), \quad (19)$$

and the Matérn correlation functions with

$$\frac{1}{\Gamma(\nu)} \left(\frac{2\sqrt{\nu}\tilde{h}}{\theta} \right)^\nu K_\nu \left(\frac{2\sqrt{\nu}\tilde{h}}{\theta} \right), \quad (20)$$

where $\tilde{h} \geq 0$ is a distance between two inputs of the GP model. $\theta > 0$ is the correlation parameter and K_ν denotes the modified Bessel function of the second kind with order ν .

Denote $\Phi_{h_k} = (\Phi_{h_k}(\|x_i - x_j\|))_{i,j=1}^n$; $\phi_{h_k}(x) = (\Phi_{h_k}(\|x - x_i\|))_{i=1}^n$ and $\mathbf{B}_{h_k} = (b_{h_k}(x_1), \dots, b_{h_k}(x_n))^T$. The posterior distribution of $h_k(\cdot)$ at an unobserved input x has the closed form [1]:

$$h_k(x)|H_n, \tilde{X}_n \sim N(\hat{h}_{k,n}(x), s_{h_k}^2(x)). \quad (21)$$

Here, the posterior mean is

$$\hat{h}_{k,n}(x) = \mathbf{b}_{h_k}^T(x)\hat{\boldsymbol{\beta}}_{h_k} + \phi_{h_k}^T(x)\Phi_{h_k}^{-1}(H_{k,n} - \mathbf{B}_{h_k}\hat{\boldsymbol{\beta}}_{h_k}), \quad (22)$$

where $\hat{\boldsymbol{\beta}}_{h_k} = (\mathbf{B}_{h_k}^T \Phi_{h_k}^{-1} \mathbf{B}_{h_k})^{-1} \mathbf{B}_{h_k}^T \Phi_{h_k}^{-1} H_{k,n}$, and the posterior variance is

$$\begin{aligned} s_{h_k}^2(x) &= \sigma_{h_k}^2 \{ \Phi_{h_k}(x, x) - \phi_{h_k}^T(x)\Phi_{h_k}^{-1}\phi_{h_k}(x) \} \\ &+ \sigma_{h_k}^2 U_{h_k}^T(\tilde{\mathbf{x}})(\mathbf{B}_{h_k}^T \Phi_{h_k}^{-1} \mathbf{B}_{h_k})^{-1} U_{h_k}(\tilde{\mathbf{x}}), \end{aligned} \quad (23)$$

where $U_{h_k}(x) = \mathbf{b}_{h_k}(x) - \mathbf{B}_{h_k}^T \Phi_{h_k}^{-1} \phi_{h_k}(x)$. Formulations of the posterior mean and posterior variance function of $g(\cdot)|D_n$ are the same as (22) and (23), respectively. In addition, the process variance $\sigma_{h_k}^2$ and the hyper-parameter θ in the correlation function are always unknown in practice, maximum likelihood estimators (MLEs) can be plugged into (21) to obtain the posterior distribution of h_k .

APPENDIX B TECHNICAL PROOFS

Proof 1 (Proof of Theorem 2):

The nested computer models $f(\tilde{\mathbf{x}})|D_n$ can be approximated by

$$Z(\tilde{\mathbf{x}}) = \mu_Z(\tilde{\mathbf{x}}) + \mathbf{c}_h^T(\tilde{\mathbf{x}})\boldsymbol{\xi}_h + c_g(\tilde{\mathbf{x}})\xi_g + \mathbf{c}_{h,g}^T(\tilde{\mathbf{x}})\boldsymbol{\xi}_h \xi_g. \quad (24)$$

Because $\boldsymbol{\xi}_h \sim N(0, I_p)$, where I_p is a $p \times p$ identity matrix, we have that $\mathbf{c}_h^T(\tilde{\mathbf{x}})\boldsymbol{\xi}_h \sim N(0, s_1^2(\tilde{\mathbf{x}}))$ and $\mathbf{c}_{h,g}^T(\tilde{\mathbf{x}})\boldsymbol{\xi}_h \sim N(0, s_2^2(\tilde{\mathbf{x}}))$, respectively. Here, $s_1^2(\tilde{\mathbf{x}}) = \mathbf{c}_h^T(\tilde{\mathbf{x}})\mathbf{c}_h(\tilde{\mathbf{x}})$ and $s_2^2(\tilde{\mathbf{x}}) = \mathbf{c}_{h,g}^T(\tilde{\mathbf{x}})\mathbf{c}_{h,g}(\tilde{\mathbf{x}})$. Denote η_h to be a standard normal random variable, where the subscript h indicates that this randomness is caused by the inner GP model. Thus, $Z(\tilde{\mathbf{x}})$ can be represented as

$$\hat{g}_n \left(\hat{\mathbf{h}}_n^T(x), x' \right) + s_1(\tilde{\mathbf{x}})\eta_h + c_g(\tilde{\mathbf{x}})\xi_g + s_2(\tilde{\mathbf{x}})\eta_h \xi_g.$$

The condition $c_{h,g}(\tilde{\mathbf{x}}) \neq \mathbf{0}_{1 \times p}$ means that $s_2(\tilde{\mathbf{x}}) \neq 0$. By some numerical calculations, it is easily verified that

$$\begin{aligned} Z(\tilde{\mathbf{x}}) &= \left\{ \eta_h + \frac{c_g(\tilde{\mathbf{x}})}{s_2(\tilde{\mathbf{x}})} \right\} \times \{s_2(\tilde{\mathbf{x}})\xi_g + s_1(\tilde{\mathbf{x}})\} \\ &+ \left[\hat{g}_n(\hat{\mathbf{h}}_n^T(x), x') - c_g(\tilde{\mathbf{x}}) \frac{s_1(\tilde{\mathbf{x}})}{s_2(\tilde{\mathbf{x}})} \right]. \\ &= Z_1(\tilde{\mathbf{x}})Z_2(\tilde{\mathbf{x}}) + z_0(\tilde{\mathbf{x}}). \end{aligned}$$

Let $\mu_1(\tilde{\mathbf{x}}) = c_g(\tilde{\mathbf{x}})/s_2(\tilde{\mathbf{x}})$; $\sigma_1(\tilde{\mathbf{x}}) = 1$; $\mu_2(\tilde{\mathbf{x}}) = s_1(\tilde{\mathbf{x}})$; $\sigma_2(\tilde{\mathbf{x}}) = s_2(\tilde{\mathbf{x}})$. Then for fixed $\tilde{\mathbf{x}} \in \mathcal{X}$, $Z_1(\tilde{\mathbf{x}}) - z_0(\tilde{\mathbf{x}})$ is a random variable generated by a production of two normal variables $Z_1(\tilde{\mathbf{x}})$ and $Z_2(\tilde{\mathbf{x}})$, with $Z_1(\tilde{\mathbf{x}}) \sim N(\mu_1(\tilde{\mathbf{x}}), \sigma_1^2(\tilde{\mathbf{x}}))$ and $Z_2(\tilde{\mathbf{x}}) \sim N(\mu_2(\tilde{\mathbf{x}}), \sigma_2^2(\tilde{\mathbf{x}}))$.

The exact probability density function of $Z(\tilde{\mathbf{x}})$ can be computed as [32]:

$$p_Z(z) = \frac{\int_{-\infty}^{\infty} \frac{1}{|t|} \exp\left\{-\frac{u_1^2(t, \tilde{\mathbf{x}}) + u_2^2(z, t, \tilde{\mathbf{x}})}{2}\right\} dt}{2\pi\sigma_1(\tilde{\mathbf{x}})\sigma_2(\tilde{\mathbf{x}})}, \quad (25)$$

where $u_1(t, \tilde{\mathbf{x}}) = \frac{t - \mu_1(\tilde{\mathbf{x}})}{\sigma_1(\tilde{\mathbf{x}})}$, $u_2(z, t, \tilde{\mathbf{x}}) = \frac{z + z_0(\tilde{\mathbf{x}}) - t\mu_2(\tilde{\mathbf{x}})}{|t|\sigma_2(\tilde{\mathbf{x}})}$. The cumulative density function of $Z(\tilde{\mathbf{x}})$ is

$$P_Z(z) = \int_{-\infty}^{\infty} \frac{1}{\sigma_1(\tilde{\mathbf{x}})} \phi_N(u_1(t, \tilde{\mathbf{x}})) \Phi_N(u_2(z, t, \tilde{\mathbf{x}})) dt. \quad (26)$$

Because $Z_1(\tilde{\mathbf{x}})$ is independent from $Z_2(\tilde{\mathbf{x}})$, mean function and variance function of $Z(\tilde{\mathbf{x}})$ can be easily deduced:

$$\begin{aligned} E[Z(\tilde{\mathbf{x}})] &= E[Z_1(\tilde{\mathbf{x}})] \times E[Z_2(\tilde{\mathbf{x}})] + z_0(\tilde{\mathbf{x}}), \\ &= \mu_1(\tilde{\mathbf{x}})\mu_2(\tilde{\mathbf{x}}) + z_0(\tilde{\mathbf{x}}). \\ \text{Var}[Z(\tilde{\mathbf{x}})] &= E[Z_1^2(\tilde{\mathbf{x}})] \times E[Z_2^2(\tilde{\mathbf{x}})] - \mu_1^2(\tilde{\mathbf{x}})\mu_2^2(\tilde{\mathbf{x}}), \\ &= [\sigma_1^2(\tilde{\mathbf{x}}) + \mu_1^2(\tilde{\mathbf{x}})] [\sigma_2^2(\tilde{\mathbf{x}}) + \mu_2^2(\tilde{\mathbf{x}})] - \{\mu_1^2(\tilde{\mathbf{x}})\mu_2^2(\tilde{\mathbf{x}})\}, \end{aligned}$$

which implies the desired results.

Proof 2 (Proof of Theorem 4): Based on the definition of NEI function (14), we have

$$\text{NEI}_n(\tilde{\mathbf{x}}) \approx E_Z(f_n^* - Z(\tilde{\mathbf{x}}))_+. \quad (27)$$

Let $U = f_n^* - Z(\tilde{\mathbf{x}})$, we can rewrite $\text{NEI}_n(\tilde{\mathbf{x}})$ as

$$\frac{1}{\sqrt{2\pi}\sigma_1(\tilde{\mathbf{x}})} \int_{-\infty}^{\infty} \exp\left\{-\frac{1}{2} \times \frac{(t - \mu_1(\tilde{\mathbf{x}}))^2}{\sigma_1^2(\tilde{\mathbf{x}})}\right\} B(t) dt, \quad (28)$$

where $B(t) = \int_0^{\infty} \frac{u}{|t|\sqrt{2\pi}\sigma_2(\tilde{\mathbf{x}})} \exp\left\{-\frac{1}{2} \times \left[u_2' - \frac{\mu_2(\tilde{\mathbf{x}})}{\sigma_2(\tilde{\mathbf{x}})}\right]^2\right\} du$, and $u_2' = \frac{f_n^* - u - z_0(\tilde{\mathbf{x}}) - t\mu_2(\tilde{\mathbf{x}})}{|t|\sigma_2(\tilde{\mathbf{x}})}$. By some easy numerical calculations, we have that,

$$\begin{aligned} B(t) &= [f_n^* - z_0(\tilde{\mathbf{x}}) - t\mu_2(\tilde{\mathbf{x}})] \Phi_N(u_2(f_n^*, t, \tilde{\mathbf{x}})) + \\ &|t|\sigma_2(\tilde{\mathbf{x}})\phi_N(u_2(f_n^*, t, \tilde{\mathbf{x}})). \end{aligned} \quad (29)$$

Substituting (29) into (28), the desired results then can be obtained.

APPENDIX C

CHOICE OF THE CORRELATION FUNCTIONS

In this section, we illustrate the reasons that we choose Matérn correlation functions (20) as the correlation functions in the numerical studies.

We compared the prediction accuracy of the one-GP model and the NGP model in the example IV-A with different correlation functions:

- Gaussian (Radial Basis Function) Kernel: $\exp(-\theta h^2)$;
- Exponential Kernel: $\exp(-\theta h)$;
- Power-exponential Kernel: $\exp(-\theta h^p)$, $p > 0$;
- Matérn correlation function (20) with $\nu = \frac{3}{2}$;
- Matérn correlation function with $\nu = \frac{5}{2}$.

Here, $h \geq 0$ is a distance between two inputs of the GP model. $\theta > 0$ is the correlation parameter which can be estimated by the maximum likelihood method. Figure 14-18 compare the accuracy of one-GP and NGP models with different correlation functions.

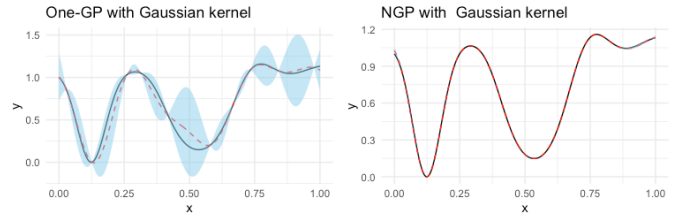


Fig. 14. Left: predictions (red dotted line) and 95% confidence intervals of the one-GP model build by using $(\tilde{X}_{n_0}, Y_{n_0})$, with $n_0 = 10$; Right: predictions (red dotted line) and 95% confidence intervals of the NGP model.

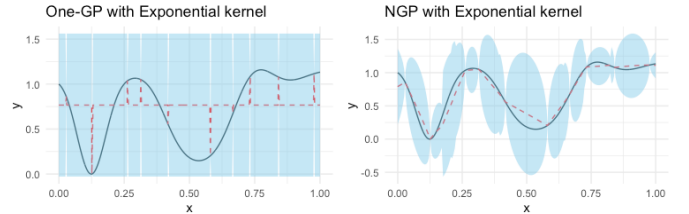


Fig. 15. Predictions (red dotted line) and 95% confidence intervals (blue interval) of the one-GP model (left) and the NGP model (right).

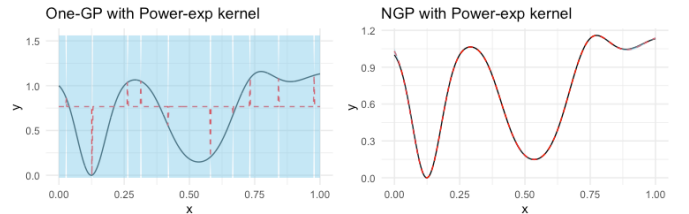


Fig. 16. Predictions (red dotted line) and 95% confidence intervals (blue interval) of the one-GP model (left) and the NGP model (right), with the parameter $p = 1.96$.

From Figure 14- 18, we can see that, with the same kernel, the NGP model outperforms the one-GP model. Since the covariance matrix obtained by using the Gaussian correlation function is prone to be a singular matrix, we did not use

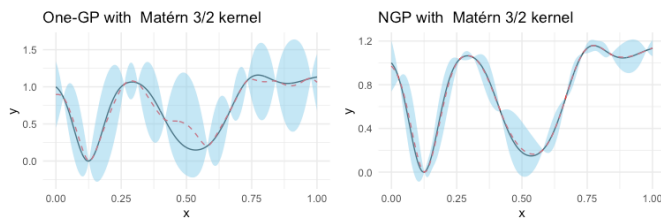


Fig. 17. Predictions (red dotted line) and 95% confidence intervals (blue interval) of the one-GP model (left) and the NGP model (right).

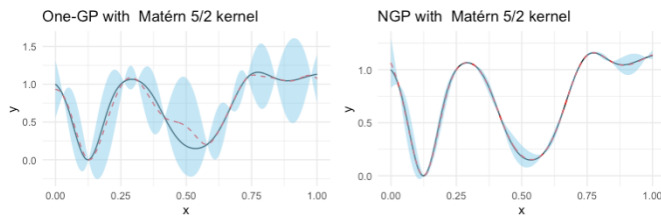


Fig. 18. Predictions (red dotted line) and 95% confidence intervals (blue interval) of the one-GP model (left) and the NGP model (right).

the Gaussian correlation function in this paper. By taking the prediction accuracy of both the one-GP and the NGP models into account, we recommend choosing the Matérn correlation functions (20).